48th AIAA Aerospace Sciences Meeting Including the New Horizons Forum and Aerospace Exposition
4 - 7 January 2010, Orlando, Florida

AIAA 2010-1525

Turbulence-Chemistry Interaction and Heat Transfer Modeling of H_2/O_2 Gaseous Injector Flows

Emre Sozer[*], Ez A. Hassan[†], Seokjun Yun[‡]
University of Michigan, Ann Arbor, MI

Siddharth Thakur [§] and Jeffrey Wright[**]
Streamline Numerics, Inc., Gainesville, FL 32609

Matthias Ihme[††] and Wei Shyy[‡‡]
University of Michigan, Ann Arbor, MI

Abstract

Reliable prediction of rocket injector flows introduces significant challenges associated with the complex physics involving recirculation, turbulence, scalar mixing, chemical reactions and wall heat transfer. This work is aimed at assessing the importance of turbulence-chemistry interaction and non-equilibrium effects in experimentally characterized single and multi-element injector flows. By examining the different chemistry models (laminar finite rate, assumed PDF with either flamelet or equilibrium assumption), it was found that for both cases investigated, chemical non-equilibrium is insignificant while substantial turbulence-chemistry interaction is observed. A zonal wall treatment was developed based on a blend of SST low-Re turbulence wall treatment and law-of-the-wall, showing improved predictive capability. A heat flux extraction method was also proposed to estimate heat flux results from adiabatic flamelet model under the consideration that wall heat loss is small compared to the overall energy generated by chemical reactions.

Nomenclature

$\bar{\ }$	=	averaged quantity
$\sim$	=	Favre averaged quantity
$(\ )_{st}$	=	quantity at stoichiometric condition
$(\ )_w$	=	wall quantity
C_p	=	specific heat
D	=	species diffusivity
H	=	total (or stagnation) enthalpy
k	=	turbulence kinetic energy
K	=	thermal conductivity

[*] Graduate Student Research Assistant, Aerospace Engineering Department
[†] Graduate Student Research Assistant, Aerospace Engineering Department
[‡] Graduate Student Research Assistant, Aerospace Engineering Department
[§] Senior Scientist, Streamline Numerics, Inc.
[**] Senior Scientist, Streamline Numerics, Inc.
[††] Assistant Professor, Aerospace Engineering Department
[‡‡] Clarence L. "Kelly" Johnson Collegiate Professor and Chair, Aerospace Engineering Department

NS = number of species
p = pressure
Pr = Prandtl number
Pr_t = turbulent Prandtl number
q_i = heat flux vector
Sc = Schmidt's number
Sc_t = turbulent Schmidt's number
T = temperature
u_j = mean mixture velocity vector
y = normal distance from wall
Y_i = mass fraction of species i
Z = mixture fraction
Z'^2 = mixture fraction variance
δ_{ij} = Kronecker delta
μ = molecular viscosity
μ_t = dynamic eddy viscosity
ν_t = kinematic eddy viscosity
τ_{ij} = viscous stress tensor
$\dot{\omega}$ = chemical heat release source term
ν = kinematic viscosity
ρ = mixture density
χ = scalar dissipation rate
ω = turbulent specific dissipation rate

I. Introduction

THE design and analysis practice for advanced propulsion systems, particularly chemical rocket engines, relies heavily on expensive full-scale prototype development and testing. Over the past decade, the use of high-fidelity analysis and design tools based on Computational Fluid Dynamics (CFD) has been identified as one way to alleviate testing costs and to develop these devices better, faster and cheaper. A critical sub-system in the performance, life-cycle cost and robustness of the overall rocket engine is the injector. This study focuses on evaluating and improving the predictive capabilities of representative CFD modeling approaches for liquid rocket injector flows through systematic assessment of various model aspects. Table 1 summarizes selected studies based on computational modeling of single element O_2/H_2 shear coaxial injector flows.

Foust et al.[1] experimentally and numerically studied a GH_2/GO_2 single element injector with an optically accessible combustion chamber. They used the laminar finite-rate chemistry formulation together with the $k-\varepsilon$ turbulence model. In this laminar finite-rate chemistry model, effects of turbulence on reaction chemistry are neglected, resulting in convenient model simplifications. Fair qualitative agreement with measured species mole fractions and quantitative agreement with the measured velocity field were obtained while the agreement deteriorated downstream with the distance from the injector face.

Schley et al.[3] simulated the same experimental configuration of Foust et al.[1] with 3 different codes, all utilizing the laminar finite-rate chemistry formulation together with the $k-\varepsilon$ turbulence model. All three simulations used an axisymmetric domain to model the square combustion chamber. Similar turbulence and chemistry modeling used in different solvers rendered similar results within themselves and the numerical results of Foust et al.[1]. Assessment of modeling approaches was not provided.

Oefelein et al.[6] simulated a LOX/GH_2 high pressure case with a large eddy simulation (LES) model that included models for non-idealized thermodynamics and multiphase phenomena, but no comparison to experimental data was given. Oefelein[13] subsequently performed a series of simulations using LES and direct numerical simulation (DNS) techniques for fully coupled compressible governing equations to further investigate the effect of non-idealized

thermodynamics. Results showed the near jet region to be diffusion dominated with intense property gradients approaching contact discontinuity.

Ivancic et al.[8] used an equilibrium chemistry formulation with $k-\varepsilon$ turbulence model to simulate an experimental LOX/GH_2 single element injector problem. Experiments were also conducted by the authors. An axisymmetric domain and adaptive grid was used. Computed near-injector radial OH mass fraction profile was compared to the experimental values measured in gray levels. Hence a quantitative comparison was not available. OH zone thickness in the computation was not predicted correctly. Authors attributed the discrepancy to the equilibrium chemistry assumption.

Lin et al.[9] simulated the single element GO_2/GH_2 injector setup of Marshall et al[10]. Both codes used a laminar finite-rate chemistry formulation and Menter's baseline turbulence model. Authors investigated the effect of the turbulence wall treatment in wall heat flux predictions. For both codes, integrating to the wall, compared to the simulations employing law-of-the-wall, resulted in better agreement in initial rise and peak value of the wall heat flux but over prediction is observed downstream of the re-attachment point. There, the law-of-the-wall simulations yielded better agreement.

Cheng and Farmer[15] simulated laminar finite-rate and equilibrium chemistry formulations along with the $k-\varepsilon$ turbulence model to simulate two different LOX/GH_2 single element experimental setups. They used a multiphase flow model with real-fluid propellant properties. Agreement with experimental measurements of radial distribution of mean temperature at several axial locations was fair. Finite-rate and equilibrium chemistry computation results were only slightly different.

Mack et al.[18] simulated the GO_2/GH_2 single element injector configuration due to Conley et al[19]. The rectangular combustion chamber with rounded corners was simulated with a 3D, 45 degree-slice domain. The laminar finite rate chemistry formulation together with Menter's SST turbulence model was used. Combustion chamber peak wall heat flux location was correctly captured although the overall heat flux distribution was under-predicted. A grid resolution sensitivity study for a separate 2D single element injector problem was presented. Development of an oscillatory flame surface was observed with refined grids.

Tucker et al.[22] simulated the GO_2/GH_2 single element injector configuration due to Pal et al.[23] with several different codes representing different turbulent combustion modeling approaches and resolution ranging from 2D RANS method to 3D LES. The results for the wall heat flux distribution as well as the detailed flow fields largely vary. While no consistent trend in comparisons with measured wall heat flux distribution is observed with increased model fidelity and grid resolution, the 3D LES simulation with the largest grid density (about 255 million cells) resulted in a very good match.

To our knowledge, turbulence-chemistry interaction (TCI) was accounted for in both studies of Oefelein et al.[6,13] It was also considered in some of the studies presented in Tucker et al[22].

In our previous study[24], the laminar finite-rate chemistry model (LFRC) was tested with two different experimental injectors[23,25] to identify the importance of physical phenomena, numerical method and turbulence model. In this study, we focus on the case of Pal et al.[23] in which we compare the laminar finite rate chemistry model (LFRC) with the laminar flamelet model (LFM). LFRC incorporates, for each species, detailed transport and production/destruction via chemical reactions. However, the reaction rates are based only on the mean temperature and the effect of turbulent temperature fluctuations are ignored. Hence the turbulence-chemistry interaction (TCI) is not accounted for in the LFRC model. LFM, on the other hand, provides an implicit way of accounting for the TCI through use of presumed shape probability density functions (PDF).

This work is aimed at assessing the importance of turbulence-chemistry interaction and chemical non-equilibrium effects in experimentally characterized single and multi-element injector flows. By systematically examining the individual combustion modeling components (laminar finite rate, assumed PDF with either flamelet or equilibrium assumption), the roles played by chemical non-equilibrium and turbulence-chemistry interaction can be analyzed. Comparing LFRC with LFM provides a way to assess the importance of turbulence-chemistry interaction effects in these types of injector flows. To investigate chemical non-equilibrium effects, we use the assumed PDF/equilibrium model which is identical to the flamelet model in the limit of zero scalar dissipation rate. Differences in the flow between PDF/equilibrium model and SFLM point to the importance, or lack thereof, of chemical non-equilibrium.

Table 1. Select literature on CFD simulations of O_2/H_2 shear coaxial injectors.

Publication	Propellants	Test Case	Pressure (MPa)	Domain	CFD Code	Turbulence Model	Chemistry Model
Foust et al.[1]	GO_2/GH_2	Self Measurement	1.29	2D	PSU[2]	$k-\varepsilon$	Finite-rate 8 species, 18 reactions
Schley et al.[3]	GO_2/GH_2	Foust et al.[1]	1.29	2D	AS3D[4] FDNS[5] PSU[2]	$k-\varepsilon$	Finite-rate
Oefelein et al.[6]	LOX/GH_2	Mayer et al.[7]	10.1	2D	PSU[2]	LES	Finite-rate 9 species, 24 reactions
Ivancic et al.[8]	LOX/GH_2	Self Measurement	6	2D	AS3D[4]	$k-\varepsilon$	Equilibrium
Lin et al.[9]	GO_2/GH_2	Marshall et al.[10]	5.2	2D	FDNS[5] Loci-Chem[11,12]	Menter's Baseline	Finite-rate 7 species, 9 reactions
Oefelein[13]	LOX/GH_2	Oschwald et al.[14]	10.1	3D		DNS LES	Finite-rate 9 species, 19 reactions
Cheng et al.[15]	LOX/GH_2	Vingert et al.[16] Thomas et al.[17]	1 6	2D	FDNS[5]	$k-\varepsilon$	Finite-rate 6 species 9 reactions
Mack et al.[18]	GO_2/GH_2	Conley et al.[19]	2.75	3D	Loci-Stream[11,20]	Menter's Baseline	Finite-rate 6 species 9 reactions
Tucker et al.[22]	GO_2/GH_2	Pal et al.[23]	5.42	3D 3D 2D 2D 2D	- LESLIE3D - GEMS Loci-Chem[11,12]	LES LES LES URANS RANS	Finite-rate Finite-rate Flamelet Finite-rate Finite-rate

The turbulence wall treatment was previously identified[24] as a particularly important factor affecting the prediction accuracy of wall heat flux distribution. Here, we follow up by proposing a zonal turbulence wall treatment approach where we use a mix of law-of-the-wall and low-Re treatment (built into the SST turbulence model[26,27]) in an effort to improve the prediction accuracy.

Single injector simulations yield valuable insight into the flow physics and the performance of the numerical models used[24]. However, in practical liquid rocket engines, a large number of injector elements, typically arranged in concentric circles are utilized. In this study, we also simulate an experimental multi-element injector case containing seven injectors elements[28,29]. Both LFRC and LFM are used to examine the flow features along with the extent of the turbulence-chemistry interaction effects.

A major shortcoming of the LFM used herein is that the wall heat loss is not considered and adiabatic wall boundary conditions are used. In liquid rocket applications, wall heat transfer is an essential outcome of the simulations. To alleviate this difficulty, we propose a method where the adiabatic solution near the wall is represented by the law-of-the-wall formulation[30]. This is done as a post processing step in order to establish the thermal boundary layer. This can be expected to provide a reasonable estimate if the effect of the heat loss is limited to a thin layer near the wall and it does not affect the rest of the flow field significantly. LFRC simulations show that for the multi-element injector case to be presented here, the amount of the heat loss through the wall is only about 1% of the overall energy generated via the combustion. Thus the previous assumption may be invoked. The resulting wall heat distribution is presented in comparison to the LFRC outcome and experimental measurements. Near wall velocity and temperature profiles are also shown to describe the methodology in detail.

II. Governing Equations and Computational Modeling Approaches

The computational tool employed in the present study is called Loci-STREAM[20,21]. It integrates proven numerical methods for generalized grids and state-of-the-art physical models in a novel rule-based programming framework called *Loci*[11] which allows: (a) seamless integration of multidisciplinary physics in a unified manner, and (b) automatic handling of massively parallel computing. The objective is to be able to routinely simulate problems involving complex geometries requiring large unstructured grids and complex multidisciplinary physics. Loci-STREAM is a 2nd order accurate, pressure-based, Reynolds-averaged Navier-Stokes (RANS) code for unstructured grids, and is designed to handle all-speed flows (incompressible to supersonic). As such, the code is particularly suitable for solving multi-species flow in fixed-frame combustion devices.

A. Favre-Averaged Governing Equations

The Favre-averaged Navier-Stokes equations of mass continuity, momentum, energy and species transport are:

$$\frac{\partial \bar{\rho}}{\partial t} + \frac{\partial \bar{\rho} u_j}{\partial x_j} = 0 \tag{1}$$

$$\frac{\partial \bar{\rho} u_i}{\partial t} + \frac{\partial \bar{\rho} u_j u_i}{\partial x_j} = -\frac{\partial \bar{p}}{\partial x_i} + \frac{\partial}{\partial x_j}\left(\tilde{\tau}_{ij} - \overline{\rho u_i'' u_j''}\right)$$

$$\tilde{\tau}_{ij} = \mu\left(\frac{\partial u_i}{\partial x_j} + \frac{\partial u_j}{\partial x_i}\right) - \frac{2}{3}\mu\frac{\partial u_k}{\partial x_k}\delta_{ij} \tag{2}$$

$$-\overline{\rho u_i'' u_j''} = \mu_t\left(\frac{\partial u_i}{\partial x_j} + \frac{\partial u_j}{\partial x_i}\right) - \frac{2}{3}\mu_t\frac{\partial u_k}{\partial x_k}\delta_{ij} - \frac{2}{3}\bar{\rho}k\delta_{ij}$$

$$\frac{\partial}{\partial t}\left(\bar{\rho}H - \bar{p}\right) + \frac{\partial}{\partial x_j}\left(\bar{\rho} u_j H\right) = \frac{\partial}{\partial x_j}\left[\left(\frac{\mu}{Pr} + \frac{\mu_t}{Pr_t}\right)\frac{\partial h}{\partial x_j}\right] + \frac{\partial}{\partial x_j}\left(\rho\sum_{k=1}^{NS} h_k D_k \frac{\partial Y_k}{\partial x_j}\right)$$
$$+ \frac{\partial}{\partial x_j}\left[u_j\left(\mu + \mu_t\right)\left(\frac{\partial u_i}{\partial x_j} + \frac{\partial u_j}{\partial x_i} - \frac{2}{3}\frac{\partial u_k}{\partial x_k}\delta_{ij}\right)\right] + \frac{\partial}{\partial x_j}\left[\left(\mu + \frac{\mu_t}{\sigma_k}\right)\frac{\partial k}{\partial x_j}\right] \tag{3}$$

$$\frac{\partial \bar{\rho} Y_k}{\partial t} + \frac{\partial \bar{\rho} u_j Y_k}{\partial x_j} = \frac{\partial}{\partial x_j}\left[\left(\frac{\mu}{Sc_k} + \frac{\mu_t}{Sc_{t,k}}\right)\frac{\partial Y_k}{\partial x_j}\right] + \bar{\dot{\omega}}_k \qquad \mathrm{k} = 1, \mathrm{NS} \tag{4}$$

Similar to our previous study[24], equations are treated appropriately using standard RANS methods. Chemistry is treated optionally using the laminar finite rate chemistry model (LFRC). LFRC does not consider the fluctuating part of the reaction rate as determined by the Arrhenius relation. However, species diffusivities and thermal conductivity are modified using the eddy viscosity, a turbulent Schmidt number of 0.9 and a turbulent Prandtl number of 0.7. Previously[24], four different H_2/O_2 chemistry mechanisms were evaluated. It was found that the choice of chemistry mechanism has little effect on the overall solution for the injector flow types of interest. In this present study, we use a chemistry mechanism with 6 species (H_2, O_2, H, O, OH, H_2O) and 8 reactions[31]. Details of the reactions and the Arrhenius rate constants can be found in our previous study[24] and in Evans et al.[31]

To assess the importance of the turbulence-chemistry interaction (TCI), the laminar flamelet (LFM) model[32,33,34] is also employed and is explained further later. For turbulence closure, the SST[26,27] model is employed. Details of the model are given below.

B. Turbulence Model

Menter's Shear Stress Transport[26,27] model (SST) was used in the current study. SST uses the $k-\varepsilon$ model near solid walls and transitions to $k-\omega$ model away from the walls with the help of a blending function. Details of the model are given below. The averaging symbols will be dropped for simplicity.

Kinematic Eddy Viscosity

$$\nu_t = \frac{a_1 k}{\max(a_1\omega, \Omega F_{SST})} \tag{5}$$

where Ω is the absolute value of the vorticity, $a_1 = 0.31$, and the blending function F_{SST} is given by:

$$\mathrm{F_{SST}} = \tanh(\mathrm{arg}_{\mathrm{SST}}^2) \tag{6}$$

where

$$\mathrm{arg}_{\mathrm{SST}}^2 = \max\left(2\frac{\sqrt{\mathrm{k}}}{0.09\ \omega \mathrm{y}}, \frac{500\nu}{\mathrm{y}^2\omega}\right) \tag{7}$$

Turbulent Stress Tensor

$$\tau_{ij}^{'} = \mu_t(\partial_j u_i + \partial_i u_j) - \frac{2}{3}(\mu_t \partial_l u_l + \rho k)\delta_{ij} \tag{8}$$

Turbulent Kinetic Energy Equation

$$\partial_t(\rho k) + u_l \partial_l(\rho k) = \tau_{ij}^{'}\partial_j u_i - \beta^*\rho\omega k + \partial_j\left[(\mu + \mu_t\sigma_k)\partial_j k\right] \tag{9}$$

Turbulent Dissipation Equation

$$F_1 = \tanh\left(\left[\min\left(\max\left(\frac{\sqrt{k}}{0.09\omega y}, \frac{500\nu}{y^2\omega}\right), \frac{4\sigma_{\omega 2}k}{CD_{k\omega}y^2}\right)\right]^4\right)$$
$$CD_{k\omega} = \max\left(2\rho\sigma_{\omega 2}\frac{1}{\omega}\frac{\partial k}{\partial x_j}\frac{\partial \omega}{\partial x_j}, 10^{-20}\right) \tag{10}$$

$$\partial_t(\rho\omega) + u_l\partial_l(\rho\omega) = \frac{\gamma}{\nu_t}\tau_{ij}^{'}\partial_j u_i - \beta\rho\omega^2 + \partial_j\left[(\mu + \mu_t\sigma_\omega)\partial_j\omega\right] + 2(1-F_1)\rho\sigma_{\omega 2}\frac{1}{\omega}\partial_j k\partial_j\omega \tag{11}$$

Coefficients

$k-\omega$ and $k-\varepsilon$ model coefficients are blended as:

$$\phi = F_1\phi_{k\omega} + (1-F_1)\phi_{k\varepsilon} \tag{12}$$

where $\phi_{k\omega}$ are:

$$\sigma_{k1} = 0.85,\ \sigma_{\omega 1} = 0.5,\ \beta_1 = 0.075,\ \beta^* = 0.09,\ \kappa = 0.41,$$
$$\gamma_1 = \beta_1/\beta^* - \sigma_{\omega 1}\kappa^2/\sqrt{\beta^*} \tag{13}$$

and $\phi_{k\varepsilon}$ are:

$$\sigma_{k2} = 1.0,\ \sigma_{\omega 2} = 0.856,\ \beta_2 = 0.0828,\ \beta^* = 0.09,\ \kappa = 0.41,$$
$$\gamma_2 = \beta_2/\beta^* - \sigma_{\omega 2}\kappa^2/\sqrt{\beta^*} \tag{14}$$

Near Wall Turbulence Treatment

A difficulty in turbulent flow simulations arise due to the steep mean velocity and temperature (in non-adiabatic case) gradients near solid walls. Direct resolution of these gradients requires a boundary layer grid that is sufficiently fine at least in the normal direction. This in turn introduces increased computational cost. Perhaps more important is the fact that the wall dampens the turbulent fluctuations and the Reynolds number locally, requiring that the turbulence closure be revised. This requires a good handling of the local flow structures and is not a straightforward task. In the SST turbulence model, this phenomenon is handled by an empirical damping function which acts to limit the eddy viscosity based on the proximity to the wall and the value of absolute vorticity as shown in Eq.(5).

In this study, we either use the SST turbulence model directly in which case we refer to this treatment as low-Re method, or we utilize an alternative approach which we refer to as the law-of-the-wall. In the latter case, the velocity and the temperature in the first cell away from the wall are imposed directly via empirically obtained algebraic boundary layer profiles, hence avoiding the resolution requirement. The law-of-the-wall method[30] used here is valid in the viscous sub-layer, buffer and log-law layers up to a y^+ of about 100. The velocity profile parallel to the wall is calculated based on y (normal distance to the wall) as shown in Eqs.(15)-(17).

$$y^+ = u^+ + y^+_{white} - e^{-\kappa B}\left[1 + \kappa u^+ + \frac{\left(\kappa u^+\right)^2}{2} + \frac{\left(\kappa u^+\right)^3}{6}\right] \tag{15}$$

$$y^+_{white} = \exp\left[\frac{\kappa}{\sqrt{\Gamma}}\left(\sin^{-1}\left(\frac{2\Gamma u^+ - \beta}{Q}\right) - \Phi\right)\right]\exp(-\kappa\beta) \tag{16}$$

$$u^+ = \frac{u}{u_\tau},\ y^+ = \frac{u_\tau y}{\nu},\ u_\tau = \sqrt{\frac{\tau_w}{\rho}}$$

$$\kappa = 0.41,\ B = 5.5,\ \Gamma = \frac{Pr^{1/3}\ u_\tau^2}{2C_p T_w},\ \beta = \frac{q_w \nu_w}{T_w K_w u_\tau} \tag{17}$$

$$\Phi = \sin^{-1}\left(\frac{-\beta}{Q}\right),\quad Q = \left(\beta^2 + 4\Gamma\right)^{1/2},\quad y_0^+ = e^{-\kappa B}$$

Temperature distribution near the wall can then be calculated from Eq.(18).

$$T = T_w\left(1 + \beta u^+ - \Gamma\left(u^+\right)^2\right) \tag{18}$$

Implementation details of this law-of-the-wall formulation can be found in Nichols and Nelson[30].

C. Laminar Flamelet Model (LFM)

The laminar flamelet model[32,33,34] utilizes a conserved-scalar approach[35,36], in which all thermo-chemical quantities (such as species mass fraction, temperature, and other quantities) are represented in terms of a reduced number of scales, namely the mixture fraction, Z, and the scalar dissipation rate, χ. These thermo-chemical quantities are then obtained from the solution of the steady laminar flamelet equations. In order to account for the turbulence-chemistry interaction in this flamelet model, presumed shape PDF's for the mixture fraction and the scalar dissipation rate are introduced. These PDF's are then parameterized in terms of the first two moments of Z and χ, requiring the solution of additional transport equations for the mean and variance of the mixture fraction:

$$\frac{\partial \bar{\rho} Z}{\partial t} + \frac{\partial \bar{\rho} u_j Z}{\partial x_j} = -\frac{\partial}{\partial x_j}\left(\bar{\rho} D \frac{\partial Z}{\partial x_j} + \frac{\mu_t}{Sc_t}\frac{\partial Z}{\partial x_j}\right) \tag{19}$$

$$\frac{\partial \bar{\rho} Z''^2}{\partial t} + \frac{\partial \bar{\rho} u_j Z''^2}{\partial x_j} = \frac{\partial}{\partial x_j}\left(\frac{\mu_t}{Sc_t}\frac{\partial Z''^2}{\partial x_j}\right) + 2\frac{\mu_t}{Sc_t}\frac{\partial Z}{\partial x_j}\frac{\partial Z}{\partial x_j} - \bar{\rho}\chi \tag{20}$$

The mean scalar dissipation rate is obtained from an algebraic model:

$$\chi = c_\chi c_\mu \omega Z^{"2}$$
$$c_\chi = 2,\ c_\mu = 0.09 \tag{21}$$

An underlying assumption of the flamelet model is that the turbulent flame consists of an ensemble of laminar flamelets[37,38,39,40] stretched by the surrounding turbulent flow structure. Solutions for such flamelets, typically modeled as a counter diffusion flow problem, are pre-computed and parameterized with the scalar dissipation rate[33]. The resulting flamelets are mapped from the Z field into the laminar mixture composition field for each scalar dissipation rate. These are further processed by convoluting with presumed shape probability density functions (PDF's) to represent turbulent statistics. The results can be tabulated as a 3 dimensional lookup table as follows:

$$Z, Z^{"2}, \chi \rightarrow \bar{\rho}, \mu, D, Y_i, T \tag{22}$$

It should be noted that when χ approaches zero, the flamelet model becomes equivalent to the presumed PDF/equilibrium model[41]. The later is simpler and more convenient when non-equilibrium effects are negligible. The lack of non-equilibrium chemistry effects is often the case for hydrogen flames due to the fast chemistry as noted by Peters[42] referring to the experimental study by Barlow et al[43]. Correa and Shyy[44] addressed turbulent diffusion flames for both jet flows as well as complex 3D gas turbine combustor flows, using the assumed shape PDF with different chemistry models. In the PDF/equilibrium model, the equilibrium state for a given mixture fraction value can be uniquely determined from the mixture fraction variable and minimization of Gibb's free energy[44,45,46]. If chemical non-equilibrium is insignificant, then the flamelet model and the assumed PDF/equilibrium model are the same.

The PDF used in this study for convolution of Z is the widely adopted β function. Its two parameters can be related to the first two moments of Z as follows:

$$P(Z) = \frac{Z^{\alpha-1}(1-Z)^{\beta-1}}{\int_0^1 Z^{\alpha-1}(1-Z)^{\beta-1}\,dZ} \tag{23}$$

where

$$\alpha = Z\left[\frac{Z(1-Z)}{Z^{"2}} - 1\right] \tag{24}$$

$$\beta = (1-Z)\left[\frac{Z(1-Z)}{Z^{"2}} - 1\right] \tag{25}$$

On the other hand, a lognormal distribution for the $\tilde{P}(\chi)$ is assumed. This assumption is tested and verified by several authors[47,48]. The lognormal distribution for the scalar dissipation rate is then given as:

$$P(\chi_{st}) = \frac{1}{\chi_{st}\sigma\sqrt{2\pi}} \exp\left\{-\frac{1}{2\sigma^2}(\ln\chi_{st} - \mu)^2\right\} \tag{26}$$

with

$$\chi_{st} = \exp\left(\mu + \frac{1}{2}\sigma^2\right)$$
$$\chi_{st}^{"2} = \chi_{st}^2\left(\exp\sigma^2 - 1\right) \tag{27}$$

The PDF of the scalar dissipation rate is known if the σ and $\widetilde{\chi_{st}}$ are given. σ is assumed as unity[49] whereas $\widetilde{\chi_{st}}$ is obtained from Eq. (21)

III. Results and Discussion

In this study, we focus on two experimental setups. The first is a single element injector case based on the experimental setup of Pal et al.[23], and studied previously by Sozer et al[24]. The second is a multi-element injector case based on experiments by deRidder et al.[28,29]. The laminar finite rate chemistry (LFRC) and the laminar flamelet

model are systematically tested in order to quantify effects of modeling parameters and numerical settings on flame structure and flow field dynamics.

A. Single injector simulation

Computational domain and boundary condition types for the Pal et al.[23] injector are depicted in Figure 1. Axisymmetric domain is modeled with a 1-degree pie shaped grid (circumferential dimension is exaggerated in Figure 1 for clarity). For the chamber wall thermal boundary condition, either a uniform wall temperature or adiabatic boundary condition (as required by flamelet model) is used. In simulations with imposed wall temperature,

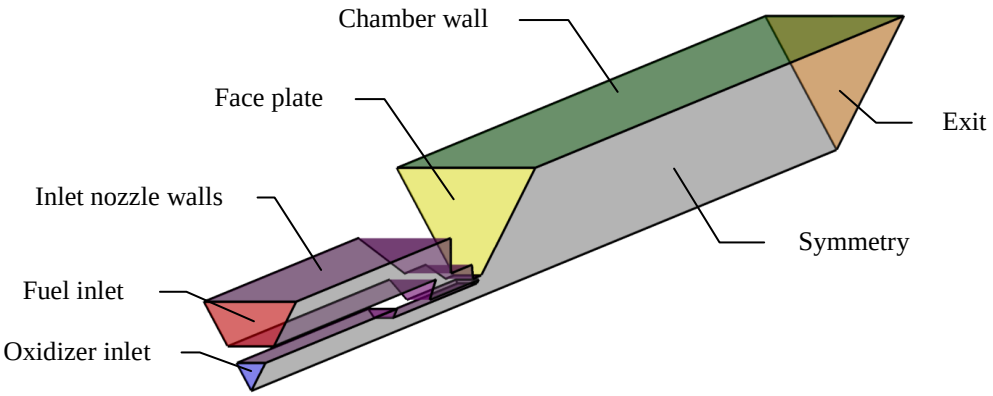

Thermal Boundary Conditions

Inlet nozzle walls	Face plate	Chamber wall
Adiabatic	Constant T=754K or adiabatic	Constant T=700 K **or a**diabatic

Figure 1. Computational domain schematic and thermal boundary conditions for Pal et al.[23] injector.

Table 2. Details of the Pal et al.[23] test case.

		Pal et al.[23]
	Oxidizer post inner diameter (mm)	5.26
	Oxidizer post thickness (mm)	1.04
	Fuel annulus diameter, D_O (mm)	7.49
	Chamber height (mm)	38.1
	Chamber length (mm)	286
Fuel	Fuel mass flux (g/s)	33.1
	H_2 mass fraction in fuel	0.402
	Velocity (m/s)	740
	Temperature (K)	811
Oxidizer	Oxidizer mass flux (g/s)	90.4
	O_2 mass fraction in oxidizer	0.945
	Velocity (m/s)	146
	Temperature (K)	700
	Equivalence ratio	1.24
	Fuel/Oxidizer velocity ratio	5.07
	Chamber pressure (bars)	54.2

face plate temperature value is set to the upstream end of the measured chamber wall temperature data whereas the chamber wall temperature value is chosen based on the measured distribution average. Effect of imposing the experimental distribution versus a uniform temperature value was explored in Sozer et al.[24] and the wall heat flux prediction was found to be only weakly sensitive to the choice.

In the flamelet model simulations, all the walls are taken to be adiabatic because of the model limitations. Furthermore, the flamelet simulations are conducted as incompressible since the individual flamelets are calculated at a constant pressure equal to the measured chamber pressure.

Turbulence-Chemistry Interaction & Chemical Non-equilibrium

In our previous study[24], it was found that when using LFRC, changing the chemistry mechanism had no noticeable effect on the overall solution suggesting that non-equilibrium effects are negligible for this case. In this study, Pal et al.[23] case is further tested with the presumed PDF/equilibrium model (achieved by setting the scalar dissipation rate to zero in the laminar flamelet model). An investigation of the effect of turbulence-chemistry interaction (TCI) is also performed by comparing the results of the laminar finite-rate chemistry model (LFRC) and the laminar flamelet model (LFM) for the Pal et al.[23] case. Because the flamelet model can only handle adiabatic thermal boundary conditions, all three cases are tested with adiabatic walls. In all simulations, identical chemistry mechanisms (6 species and 8 reactions) were used and the computational grids were also identical.

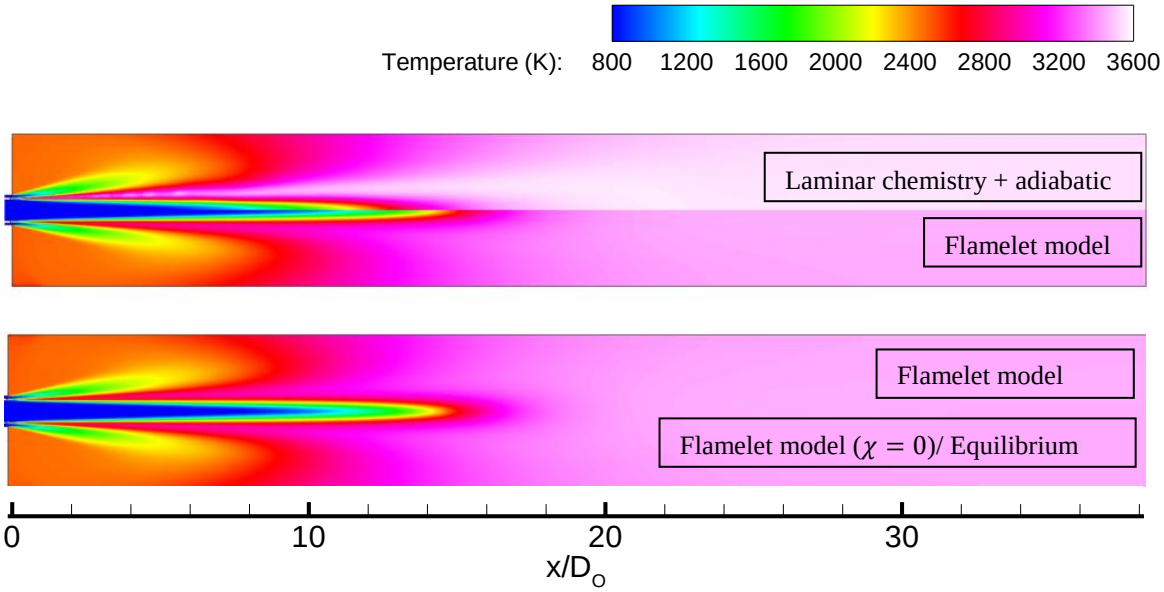

Figure 2. Comparison of temperature field results of the LFRC model and the LFM with and without the effects on chemical non-equilibrium. D_O is the fuel post outer diameter.

Temperature contours corresponding to each case are presented in Figure 2 comparatively. An immediate observation is that the flamelet model yields a consistently lower mean temperature field. The comparison will be further discussed by probing the temperature profiles at several axial locations (Figure 5) and evaluating PDF distributions at several representative points in the domain (Figure 6).

To facilitate these discussions, it is useful however to identify the contribution of the non-equilibrium chemistry effects in the flamelet model solutions first. In the limit of $\chi \to 0$, chemistry is infinitely fast compared to the diffusion and hence the propellants attain chemical equilibrium immediately upon mixing. As χ increases, diffusion time scale becomes comparable to the chemistry time scale and eventually the heat is carried out of the reaction zone at a faster rate than its generation via the chemical reactions. This in turn causes the extinguishing of the flame (quenching). In Figure 2 (bottom), the flamelet model solution is compared to the solution in which χ is taken as zero (equilibrium). In this isolated look into the effect of non-equilibrium chemistry, no identifiable difference in the temperature field is observed. In Figure 3, laminar flamelet solutions parameterized with χ_{st} are plotted. The effect

of the scalar dissipation rate is negligible for $\ln(\chi_{st}) < 8$. As shown in the mean scalar dissipation rate contours in Figure 4 as well as the values probed in Figure 6, the region where $\ln(\chi_{st}) > 8$ is confined to a small area near the injector exit where the strong shear layer between the fuel and the oxidizer streams yield a diffusive time scale small enough to interact with the chemical reaction rates. Since the non-equilibrium chemistry plays no noticeable role in the current investigation, the flamelet model essentially becomes the same as that of the assumed-PDF, chemical equilibrium model discussed in Correa and Shyy[44].

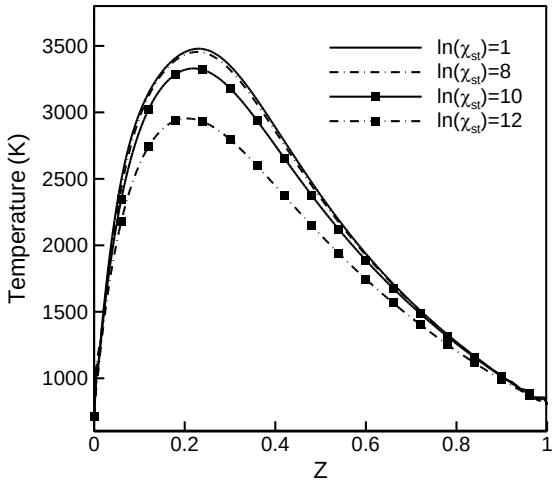

Figure 3. Laminar flamelet temperature profiles for varying stoichiometric scalar dissipation rate.

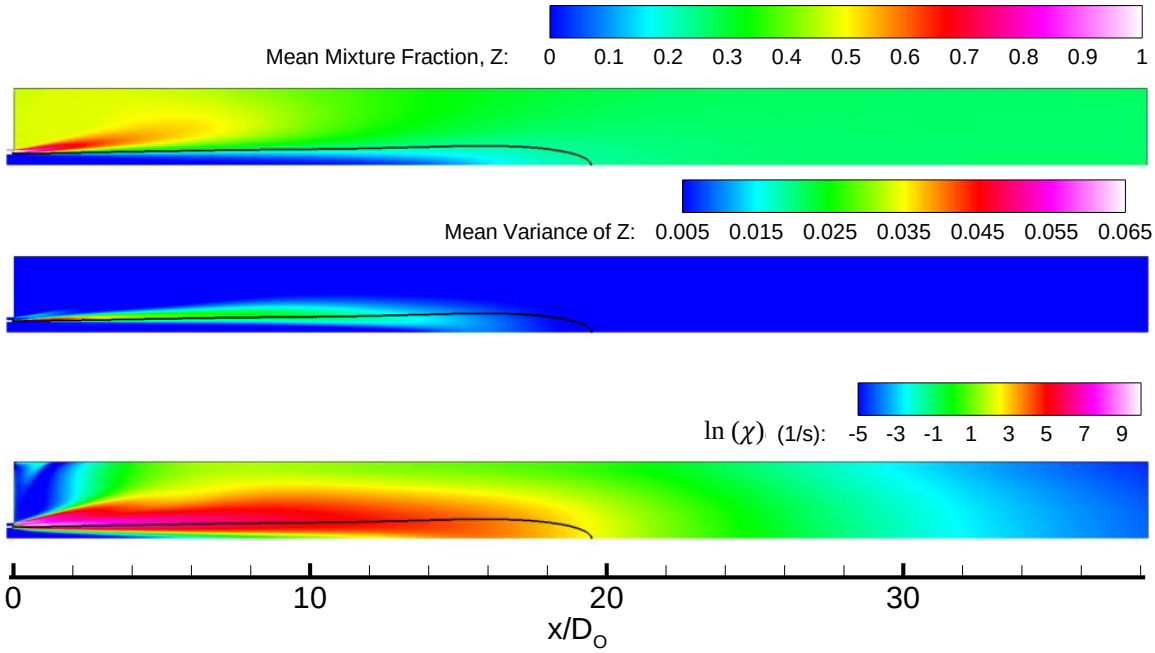

Figure 4. Flamelet model solution contours. Solid black line indicates stoichiometric mixture fraction (flame surface) at $Z_{st} = 0.229$.

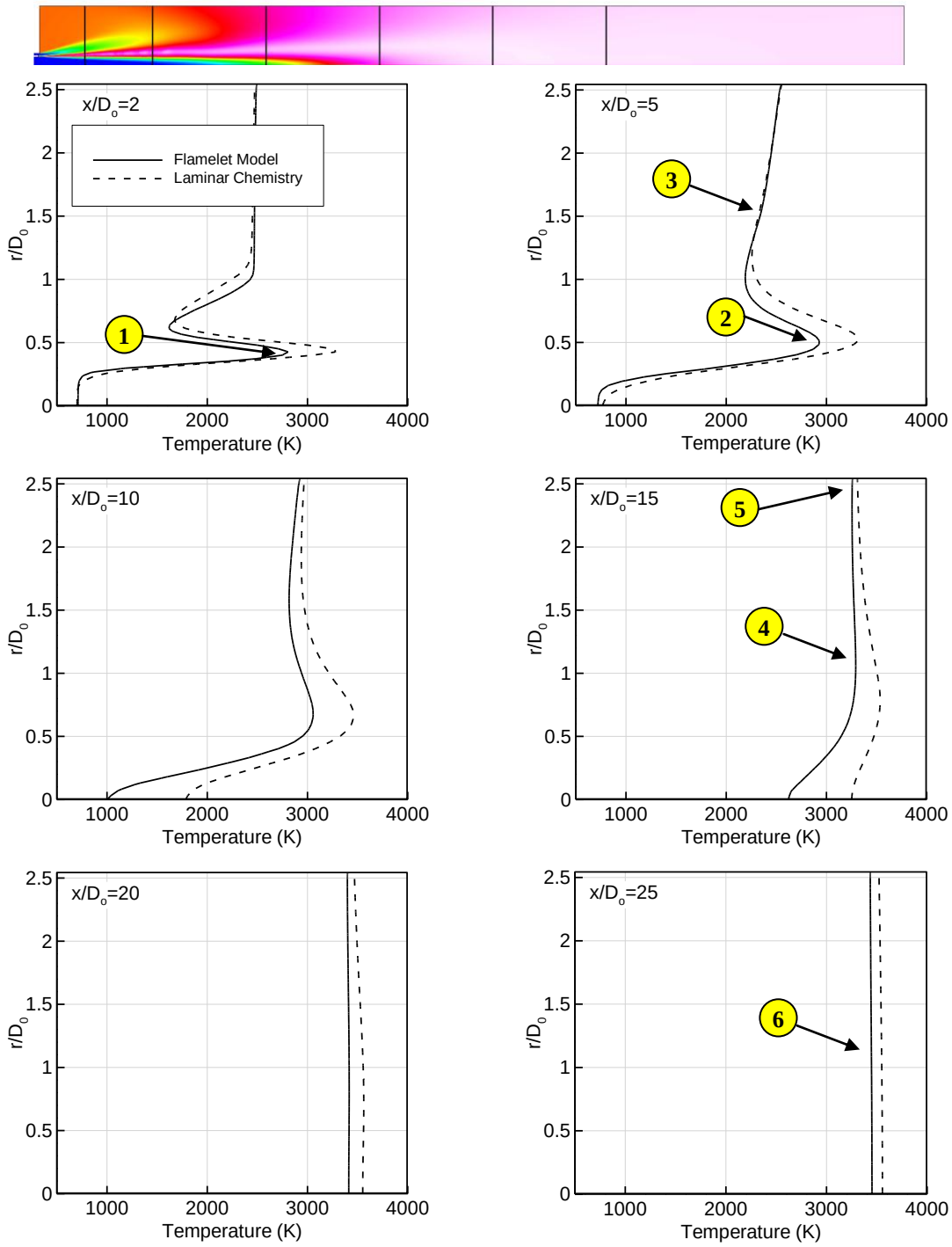

Figure 5. Comparison of temperature profiles of laminar finite rate chemistry and flamelet solutions at different axial locations. PDF distributions corresponding to the numbered locations are given in Figure 6.

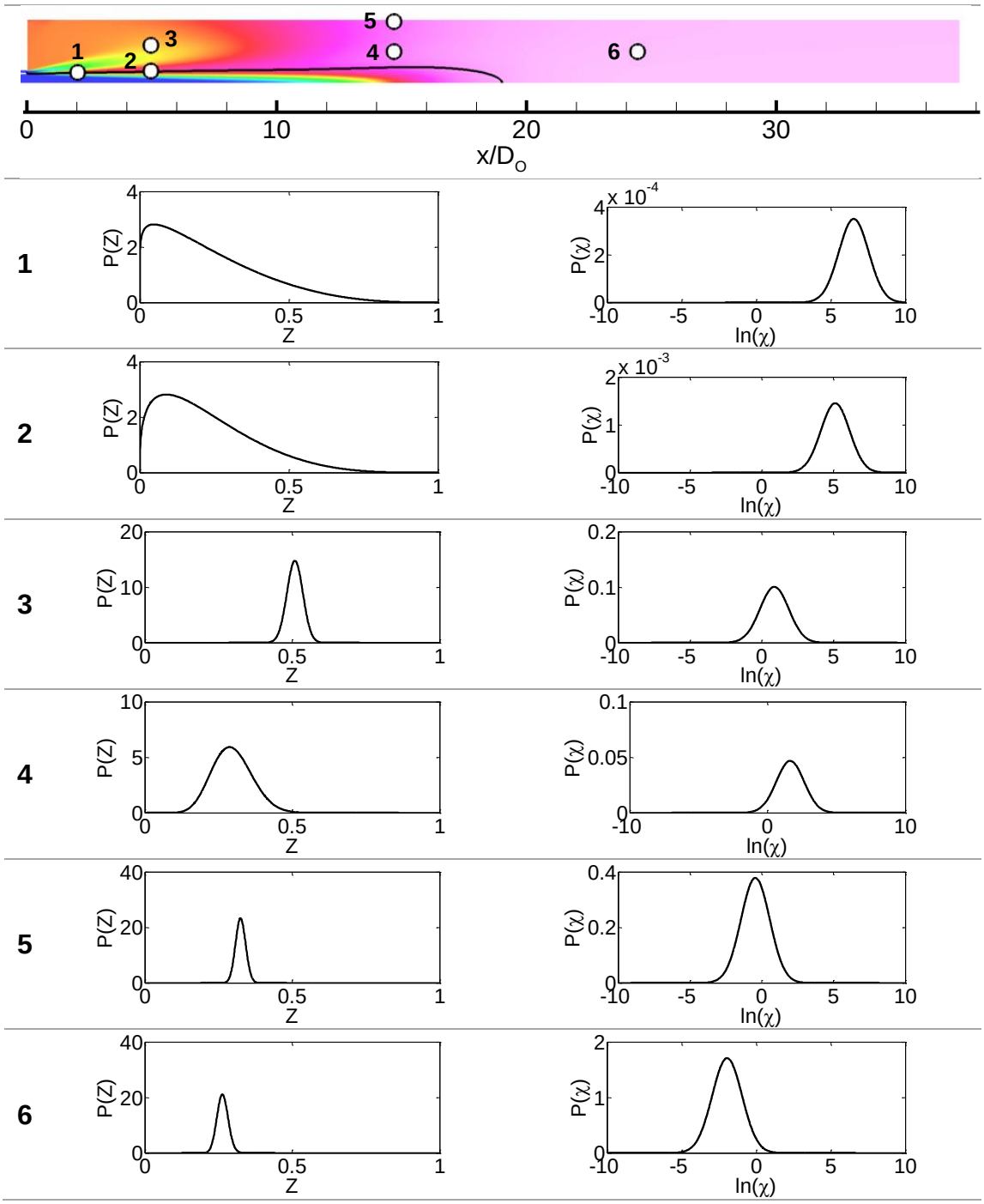

Figure 6. Probability density function (PDF) distributions of mixture fraction and scalar dissipation rate at selected points in the combustion chamber.

Radial temperature profiles at several axial locations for the laminar finite-rate chemistry (LFRC) and the laminar flamelet model (LFM) are given in Figure 5. β and lognormal PDF distributions for Z and χ corresponding to several representative points in (LFM) are given in Figure 6.

Having ruled out the effects of the scalar dissipation rate and hence the non-equilibrium chemistry in the flamelet model, the extent of the turbulence-chemistry interactions can be described by the assumed PDF distribution of the

mixture fraction Z as shown in Figure 6 and hence can be observed by comparing the LFM and LFRC simulation results in Figure 5. The skewness and width of the PDF for the mixture fraction is determined by its mean, $\tilde{Z}$, and its mean variance, $\widetilde{Z''^2}$, respectively. The mean scalar dissipation rate, $\tilde{\chi}$, is also directly related to the mean mixture fraction variance via the modeling relation given in Eq. (21). As shown in Figure 4, both $\widetilde{Z''^2}$ and $\tilde{\chi}$ are only significant near the mixing layer between fuel and oxidizer streams, and hence near the stoichiometric flame surface shown as the black line. They take their largest value upstream near the injector post tip whereas both reduce towards downstream as the mixing layer diffuses. At all x/D_0 locations, the β distribution causes a reduced temperature near the stoichiometric flame surface but slightly increased temperature away towards the wall. The effect of the PDF at this latter point (see probe point 3 in Figure 5 and Figure 6) is negligible because of the more or less uniform mixture composition and as a result, a small mixture fraction variance and hence a narrow PDF. Note that the usage of the β PDF for mixture fraction not only affects the temperature field but the density field and the distribution of the transport properties as well. Near the flame surface, a large gradient of the mixture fraction exists. Corresponding large mixture fraction variance yields a wide β PDF as shown for probe points 1 and 2. Thus the reduced peak temperature near this region is largely due to the consideration of TCI. Probe point 5 corresponds to a point near the edge of the boundary layer. There, the narrow PDF distribution points to negligible TCI effects. This holds true for any region away from the flame surface. Therefore, convergence of the temperature profiles further downstream after the closing of the flame surface is observed for locations $x/D_0 = 20, 25$.

The axial adiabatic wall temperature distributions for the laminar finite-rate chemistry (LFRC) and laminar flamelet model (LFM) simulations are given in Figure **7**. The difference in temperature is at most 3% consistent with the previous analysis because the wall is far from the flame surface.

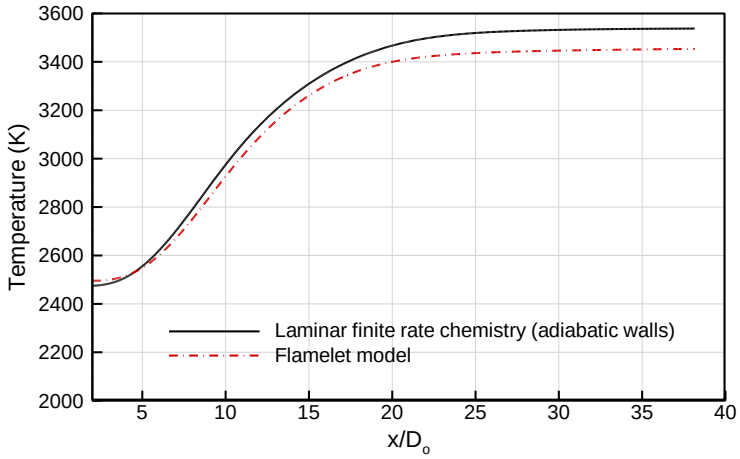

Figure 7. Adiabatic chamber wall temperature distribution for laminar finite rate chemistry and flamelet model simulations.

Zonal models for wall treatment

Sozer et al[24] have studied this case and investigated the effects of the temperature boundary condition choice, the use of different chemistry mechanisms, choice of turbulence wall treatment and grid refinement. They found that the largest variation in the wall heat flux distribution prediction was due to the choice of the law-of-the-wall versus the low-Re model.

The law-of-the-wall treatment[30] is based on an assumed velocity profile and an analogy between shear stress and heat flux. The assumed near wall velocity profile is based on the empirically observed similarity of a non-recirculating wall-bounded turbulent boundary layer flow structure. Strictly, its application to complex flow fields involving substantial flow curvatures, recirculation, and pressure gradients is invalid. The low-Re approach is conceptually more appropriate to resolve the small length scale phenomena such as shear stress and heat flux. A competing issue is that the wall dampens the turbulent fluctuation and the Reynolds number locally, requiring that the turbulence closure be revised. This requires a good handling of the local flow structures and is not a straightforward task.

Sozer et al.[24] showed that the low-Re model resulted in a better prediction of the peak wall heat flux value in the recirculating flow region before the re-attachment point whereas use of the law-of-the-wall yielded a corresponding under prediction. Further downstream after the re-attachment point, a reversal of the trend is observed consistent with the argument above; law-of-the-wall result more closely follows the experimental data and the low-Re model causes an over-prediction there.

Based on the observation in Sozer et al[24], in this study we employ a zonal wall turbulence treatment where depending on the attachment point on the chamber wall, different wall treatments are applied. Low-Re approach is applied in the upstream portion of the wall corresponding to the recirculating region. This portion is already known to extend up to $x \approx 0.1\ m$. Law-of-the-wall is applied for the rest of the chamber wall downstream where the flow is known to be attached to the wall. With the knowledge of re-attachment point location, a new blended grid was created with fine near wall spacing at the recirculation zone and coarser near wall mesh elsewhere where the law-of-the-wall is applied. The grid is shown in Figure 8.

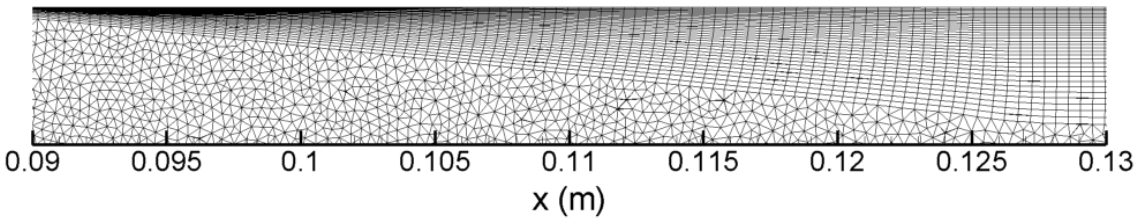

Figure 8. Boundary layer discretization, zonal treatment grid.

Results are shown in Figure 9 in comparison to the experimental data. The zonal treatment result is in well agreement to the measurements throughout the entire wall heat flux profile. However, a discontinuity in the slope of the heat flux curve is observed. This is due to the abrupt switch from the low-Re model to the law-of-the-wall treatment occurring at the point of unity y^+ for the first grid cell center off the wall.

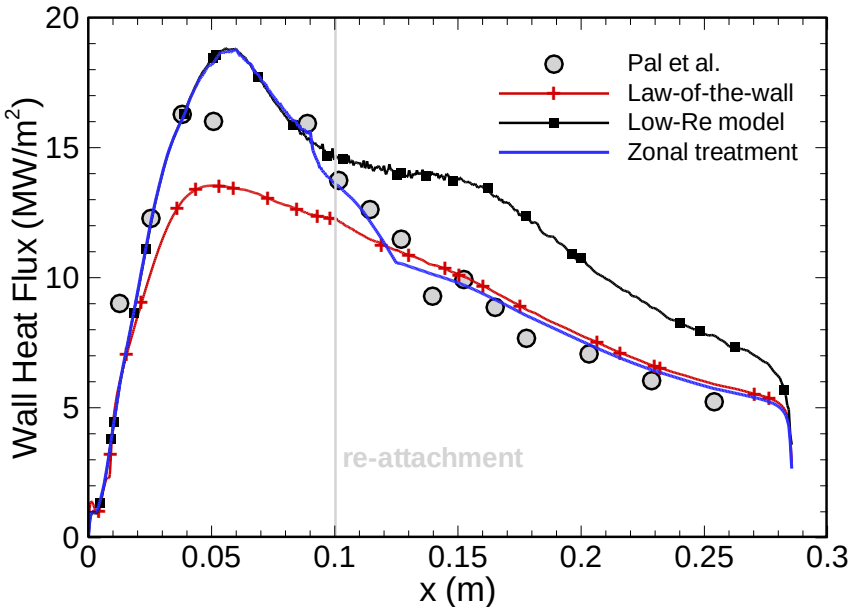

Figure 9. Effect of turbulence wall treatments on the chamber wall heat flux profile.

The zonal wall treatment option improves the heat flux predictions considerably. But in the current application, a-priori knowledge of the re-attachment point location and a new corresponding blended wall grid were needed. This issue is only an artifact of the model implementation and can be eliminated with the introduction of a boundary

condition which would enforce the use of the law-of-the-wall regardless of how low the y^+ value is. The detection of the re-attachment point location, and hence the point of switch between alternate wall treatments, can be automated. Furthermore, a blending of the two models can be applied near the switch to ensure a smooth transition.

B. Multi-element Injector Simulation

An experimental 7-element H_2/O_2 injector due to deRidder et al.[28,29] is studied and the simulation outcome is compared to the measured wall heat flux distribution. Exploiting the symmetric nature of the problem, a $1/12^{th}$ slice of the combustor is modeled which includes a $1/12^{th}$ section of the core element and a half of an outer element. Details of the computational domain and boundary conditions as well as the experimental case details are provided in Figure 10 and Table 3 respectively.

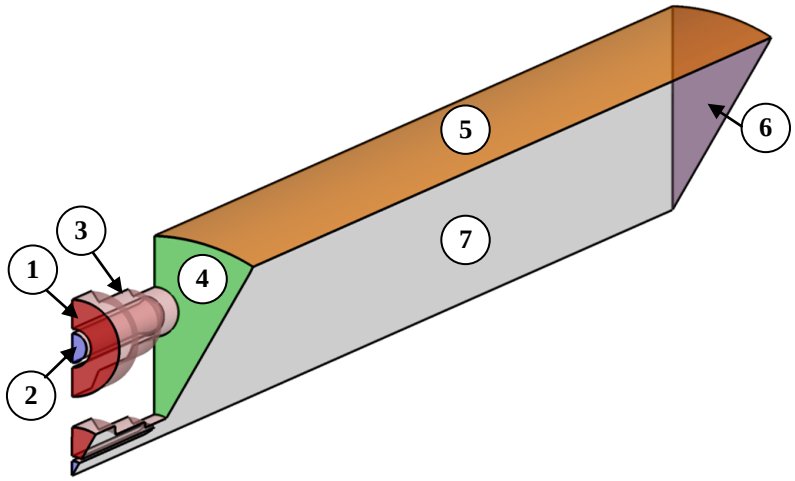

Label	Condition
1	Fuel inlet
2	Oxidizer inlet
3	Injector nozzle walls: No-slip, adiabatic
4	Face plate: No-slip @ 450 K\adiabatic
5	Chamber wall: No-slip @ 750 K\adiabatic
6	Outlet: Supersonic, extrapolated
7	Symmetry

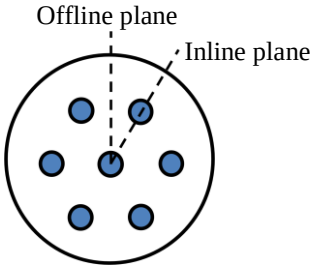

Figure 10. Computational domain and boundary conditions for the multi-injector case due to deRidder et al.[28,29]

Table 3. Multi-element injector test case details.

		deRidder et al.[28,29]
	Oxidizer post inner diameter (mm)	4.93
	Fuel post inner diameter (mm)	6.50
	Fuel post outer diameter, D_O (mm)	8.28
	Outer elements row radius (mm)	21.34
	Chamber radius (mm)	34.04
	Chamber length (mm)	307
Fuel	Total fuel mass flux (g/s)	374.2
	H_2 mass fraction in fuel	1
	Temperature (K)	300 K
Oxidizer	Total oxidizer mass flux (g/s)	1134
	O_2 mass fraction in oxidizer	1
	Temperature (K)	90 K
	Equivalence ratio (O/F)	3.03
	Chamber pressure (bars)	56.7

A 3D mixed structured/unstructured grid consisting of about 1.2 million cells is used. Boundary layer type stretched hexahedral elements are utilized near the chamber wall and the injector nozzle walls. Sample views of the grid are shown in Figure 11.

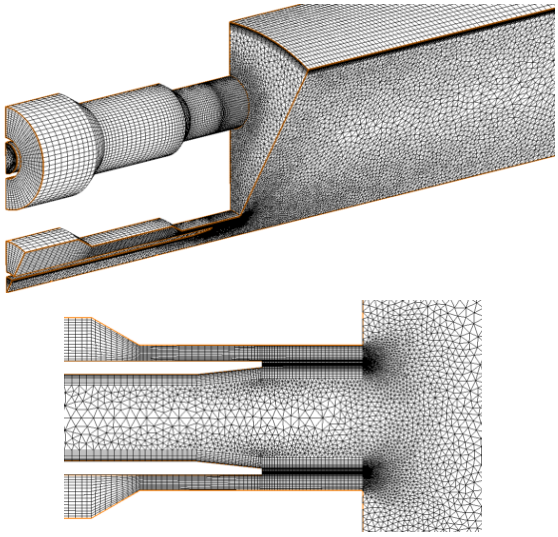

Figure 11. Top: Partial 3D view of the grid. Bottom: Cut-plane detail of the injector element post.

Flow field based on different combustion models

In the single element injector case studied so far, the turbulence-chemistry interaction effect was shown to be constrained to the near flame surface region and the wall heat flux was essentially unaltered by the effect. In a more realistic injector, large number injector elements are typically placed in patterned formation on the face plate. A commonly used arrangement is to place the elements in concentric circular rows. The result is, compared to the

single element injectors, a closer proximity of the outer row flame to the chamber wall surface. In the current multi-element injector study, the focus is hence to investigate the significance of the turbulence-chemistry interactions on the flow field in general and the near wall region in particular. The multi-element injector setup is tested with both LFRC and LFM. In the case of LFM, adiabatic boundary conditions are used on all surfaces as required by the model. The fixed temperature boundary condition is used when LFRC is employed. LFRC results predict that only 1% of the reaction generated heat is lost through the walls. Thus, even though the two cases have different wall boundary conditions, it is expected that the thermal boundary conditions will have a minimal effect on the overall solution.

Temperature contours in the inline, intermediate and offline planes for each model simulations are shown in Figure 12. Figure 14 shows the temperature contours at several axial plane slices as well as the streamline structure. In both figures, solid black lines indicate the stoichiometric flame surface ($Z = 0.111$). Overall, the temperature fields obtained from the laminar finite-rate chemistry model and the laminar flamelet model are in good agreement. However, the latter results in reduction of temperature near the flame surface due to the accounting of turbulence-chemistry interactions through presumed shape probability density functions for the mixture fraction and the scalar dissipation rate. The mean mixture fraction, its mean variance and the mean scalar dissipation rate fields are shown in Figure 15. Note that although not explicitly shown here, the scalar dissipation rate becomes significantly large only in a small region near the injector posts and thus the non-equilibrium chemistry effect is negligible elsewhere. These immediate observations are consistent with the findings with regard to the single element injector where a more in-depth comparison of the two models is provided.

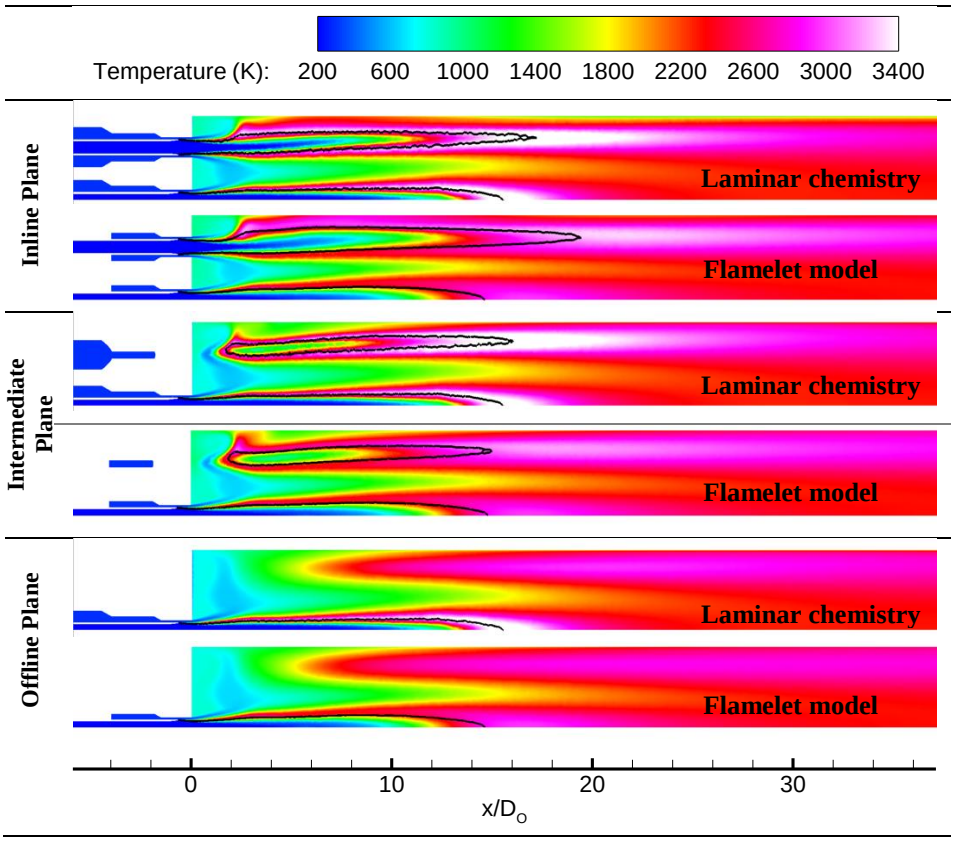

Figure 12. Inline, intermediate and offline plane temperature contours for laminar finite-rate chemistry and laminar flamelet model computations. Solid black lines indicate the stoichiometric mixture ($Z = 0.111$). D_O is the fuel post outer diameter.

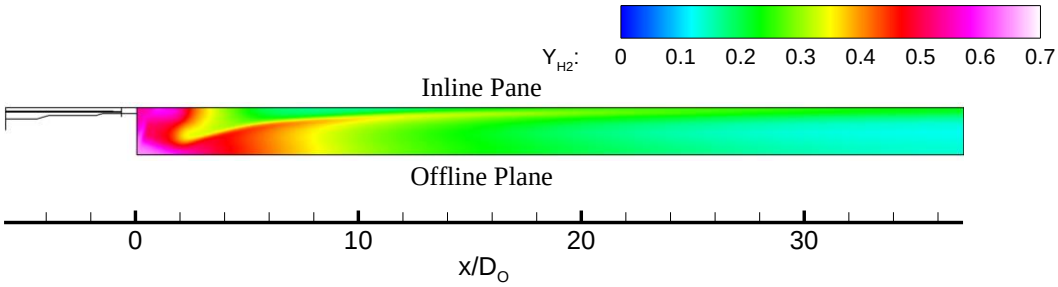

Figure 13. H_2 mass fraction contours along the chamber wall for the laminar finite-rate chemistry simulation.

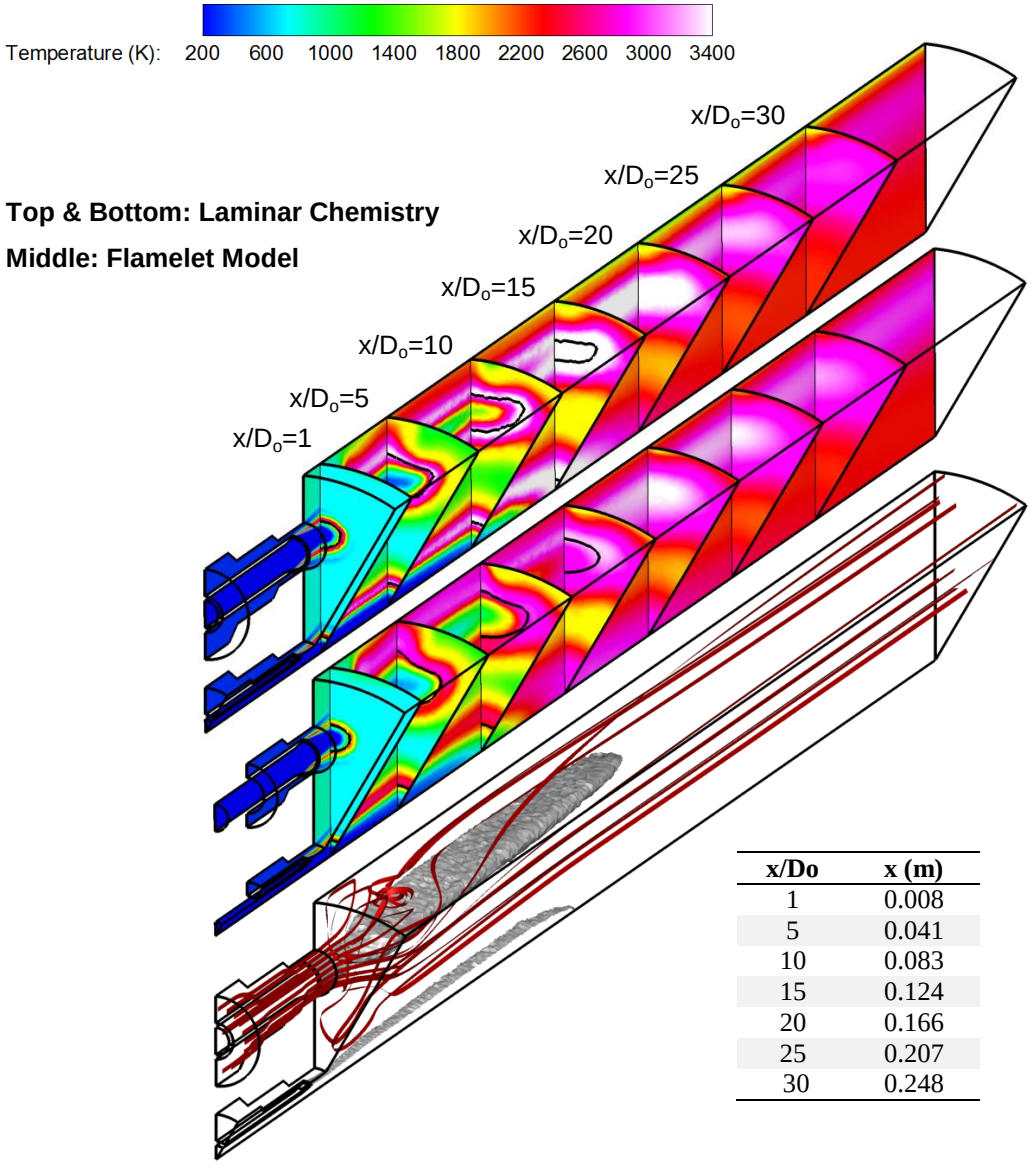

x/Do	x (m)
1	0.008
5	0.041
10	0.083
15	0.124
20	0.166
25	0.207
30	0.248

Figure 14. Temperature contours for axial plane slices. Bottom plot shows the streamline ribbons and the stoichiometric flame surface. Solid black lines indicate the stoichiometric mixture ($Z = 0.111$).

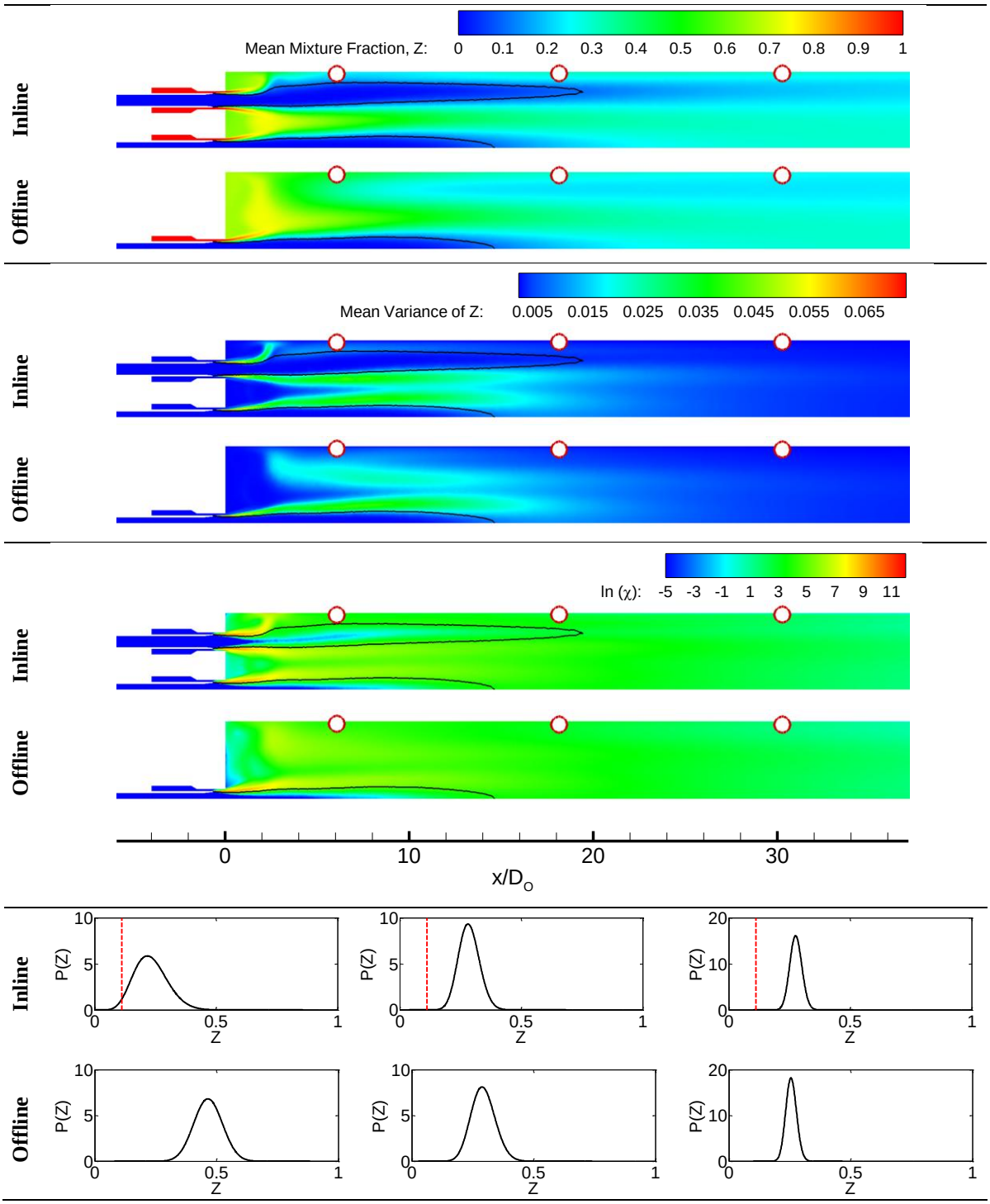

Figure 15. Contour plots for the mean mixture fraction, its mean variance and the scalar dissipation rate in the inline and offline planes and the corresponding mixture fraction PDF distributions at marked locations of x=0.05,0.15,0.25 in meters. Black line corresponds to the stoichiometric flame surface, $Z = 0.111$.

The streamlines shown in Figure 14 (bottom) mostly originate from the upper injector element fuel stream. While a portion of the fuel stream is entrained to the recirculation region between the wall and the injector jet, some

escape near the offline symmetry plane and merge to the inline plane further downstream. This fuel rich corridor is shown more clearly in Figure 13. This effect can also be observed in the temperature contours where a relatively cool layer merges to the inline plane and subsequently diffuses and diminishes further downstream. Note that this layer is thinner and faster diffusing in the flamelet model simulation. Consequently, an increased near wall temperature (compared to laminar finite-rate chemistry simulation) in the vicinity of the inline plane is realized with the flamelet model.

Consistent with the single injector results when using the flamelet model, the effect of turbulence-chemistry interactions is significant mostly near the flame surface and especially near the injector exit where the shear layer between fuel and oxidizer is stronger. The extent of the significance of turbulence-chemistry interaction is directly correlated with the mean variance of the mixture fraction, $\widetilde{Z''^2}$, as it determines the width of the probability density function of the mixture fraction. Contour plots of $\tilde{Z}$, $\widetilde{Z''^2}$ and $\tilde{\chi}$ for the inline and offline planes as well as the Z PDF distributions at select points near the wall are shown in Figure 15. In both the inline and the offline planes, the PDF width decreases towards downstream. At $x = 0.15\ m$ towards the closing of the near wall flame, and at $x = 0.25\ m$ further downstream, the PDF width is still significant. Despite the significant spread, the mean value of the mixture fraction, Z, at all locations are away from the stoichiometric value of 0.111 (shown as dashed red line in the PDF plots). Thus the influence of the PDF, and hence the local turbulence-chemistry interaction effects, near the wall are small. For the widest PDF shown in Figure 15 occurring in the inline plane upstream location, local temperature reduction due to the PDF is about 8 K (0.3%).

The axial distribution of the combustion chamber wall heat flux along the inline, offline and intermediate planes are shown in Figure 16 in comparison to the experimental measurements by deRidder et al.[28,29]. The left column, on the other hand, shows the axial distribution of temperature along a near wall line with an offset of 4 mm from the wall. The methodology to estimate the wall heat flux for the flamelet model solution is proposed in the following section. In the heat flux profiles for inline and intermediate planes, both laminar chemistry and flamelet model results show two dips roughly occurring at axial positions $x = 0.018\ m$ and $x = 0.038\ m$. These correspond to the closure of primary and secondary near wall recirculation zones as shown in Figure 14. The secondary recirculation zone does not extend up to the offline symmetry plane and hence only one dip in the heat flux curve is observed. Note that the law-of-the-wall near wall treatment was used for the laminar chemistry simulation. The flamelet model solution, on the other hand, was computed using the low-Re near wall model but the heat flux distribution was estimated as a post processing step utilizing the law-of-the-wall formulation. The law-of-the-wall method loses its validity in regions where a near wall recirculation zone or large streamline curvatures exist. Also, as for the case of the single element injector, under prediction of the heat flux in these regions is expected. The under prediction in the intermediate plane extends up to $x = 0.13\ m$ whereas quantitative agreement with the experimental data is achieved somewhat earlier for the offline plane. This is in direct correlation with aligning of the streamlines with the wall as seen in Figure 14. In the inline plane, the additional influence of the cooling due to the fuel rich layer is seen as discussed earlier. The size and the extent of this layer are predicted differently with the laminar chemistry and flamelet models. The thinner layer resulting from the flamelet model simulations translates into an overall larger near wall temperature distribution in the inline plane (Figure 16, top row, left). The outcome is that the laminar chemistry model consistently under predicts the heat flux by 30-40% compared to the experimental measurements. The flamelet model, on the other hand, was able to reproduce the experimental distribution fairly well downstream of the recirculating regions. Common to both the intermediate and the offline planes, the flamelet model wall heat flux distribution shows an increasing trend towards downstream. This stems from the current methodology for the heat flux estimation as discussed in the following section.

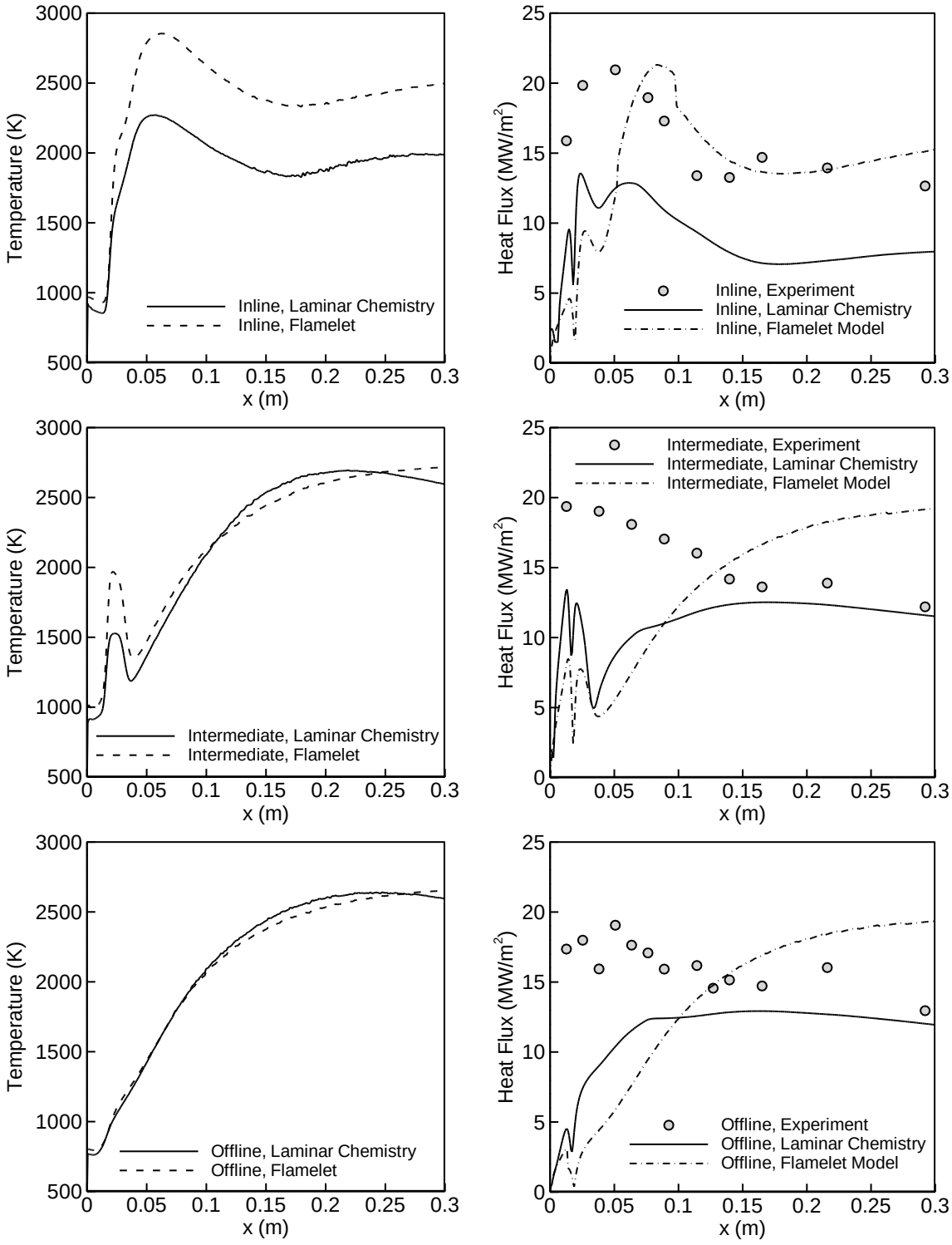

Figure 16. Spatial distribution of combustion chamber wall heat flux, computed and experimental[28].

Heat flux extraction for the flamelet model

As mentioned earlier, the current formulation of the laminar flamelet model does not account for wall heat transfer effects. However, the simulation results of the laminar finite-rate chemistry model suggest that the total heat losses to the walls amount to only 1% of the heat generated via the reactions for the multi-element injector case under consideration. Thus, it can be expected that the effect of the wall heat losses is constrained to a thin region near the boundary. The temperature field plots shown in Figure 12 qualitatively support this view.

In this case, using the computed near wall velocity and adiabatic wall temperature information, law-of-the-wall formulation can be utilized to construct the temperature gradient based on an assumed wall temperature and hence a wall heat flux value can be obtained. The procedure can be summarized in the following steps:

- Axial velocity, density and temperature values at a few grid points off the wall as well as distance to the wall are extracted from the flamelet model solution.
- Mixture fraction variable is extracted at the wall and material properties (μ, λ, C_p) are calculated based on the extracted mixture composition and an assumed wall temperature.
- Based on the information obtained in the previous steps, law of the wall formulation given in Eqs. (15)-(18) is iteratively solved to construct a near wall temperature distribution and hence the wall heat flux.

In the current study, the 3rd grid node away from the wall is used in the first step. A temperature of 750 K and a Prandtl number of 0.7, consistent with the conditions for the laminar finite rate chemistry model computation, are used at the wall. The selection of the 3rd grid point at all axial locations is somewhat arbitrary and may results in inconsistencies for the following reasons:

By using the 3rd point off the wall, a part of the velocity field solution between the wall and the 3rd grid node is being discarded and instead it is being replaced with the law-of-the-wall formula. Also, in recirculating flow regions or in regions where there is significant streamline curvature or pressure gradient near the wall, law-of-the-wall method loses its validity due to the empirical nature of the formulation. Thus it is desirable to incorporate as much of the resolved flow information as possible by choosing the 1st grid point off the wall as a basis for constructing the law-of-the-wall profiles.

An adiabatic wall boundary condition is used with the flamelet model. Hence the normal temperature gradient at the wall is zero. To construct the temperature profile with the law-of-the wall, the temperature value at the wall and at an additional point away from the wall need to be given. The wall value is assumed to be 750 K. For the second value, computed temperature at the 3rd grid point off the wall is taken. This is in effect assuming that all or most of the temperature variation due to wall heat loss occurs in 3 cell heights distance from the wall. Considering the relatively small total heat loss to the wall for the current case, this assumption might be reasonable.

In view of these discussions, the rationality of the choice of the 3rd grid point can be assessed by examining the near wall velocity and temperature profiles of the flamelet model solution as well as the profiles reconstructed with the law-of-the-wall. Near wall temperature profile resulting from the laminar finite-rate chemistry model solution can also aid in the discussion. These profiles at two different axial positions in the inline and the offline planes are provided in Figure 17.

Note that despite the y^+ number of over 20 for the first grid point, the law-of-the-wall implementation is not available for the flamelet model and hence the low-Reynolds number model was used, therefore, the near wall velocity profiles for the flamelet model solutions and those calculated afterwards via the law-of-the-wall are not expected to match identically. However, good agreement is obtained as shown in Figure 17. Moreover, the temperature profiles of the laminar finite-rate chemistry solution show that the temperature variation due to wall heat loss is largely contained within the first 3 grid points. The largest violation of this occurs at the downstream profile at the offline plane where an additional 15% temperature increase occurs between the 3rd and the 10th grid points. This can explain the overestimation of the wall heat flux at downstream locations in the intermediate and offline planes as seen in Figure 16. Ideally, rather than using a fixed height point of reference for the law-of-the-wall evaluations (such as the 3rd grid point) at all axial locations, a local selection of this point can be made based on the local velocity boundary layer height.

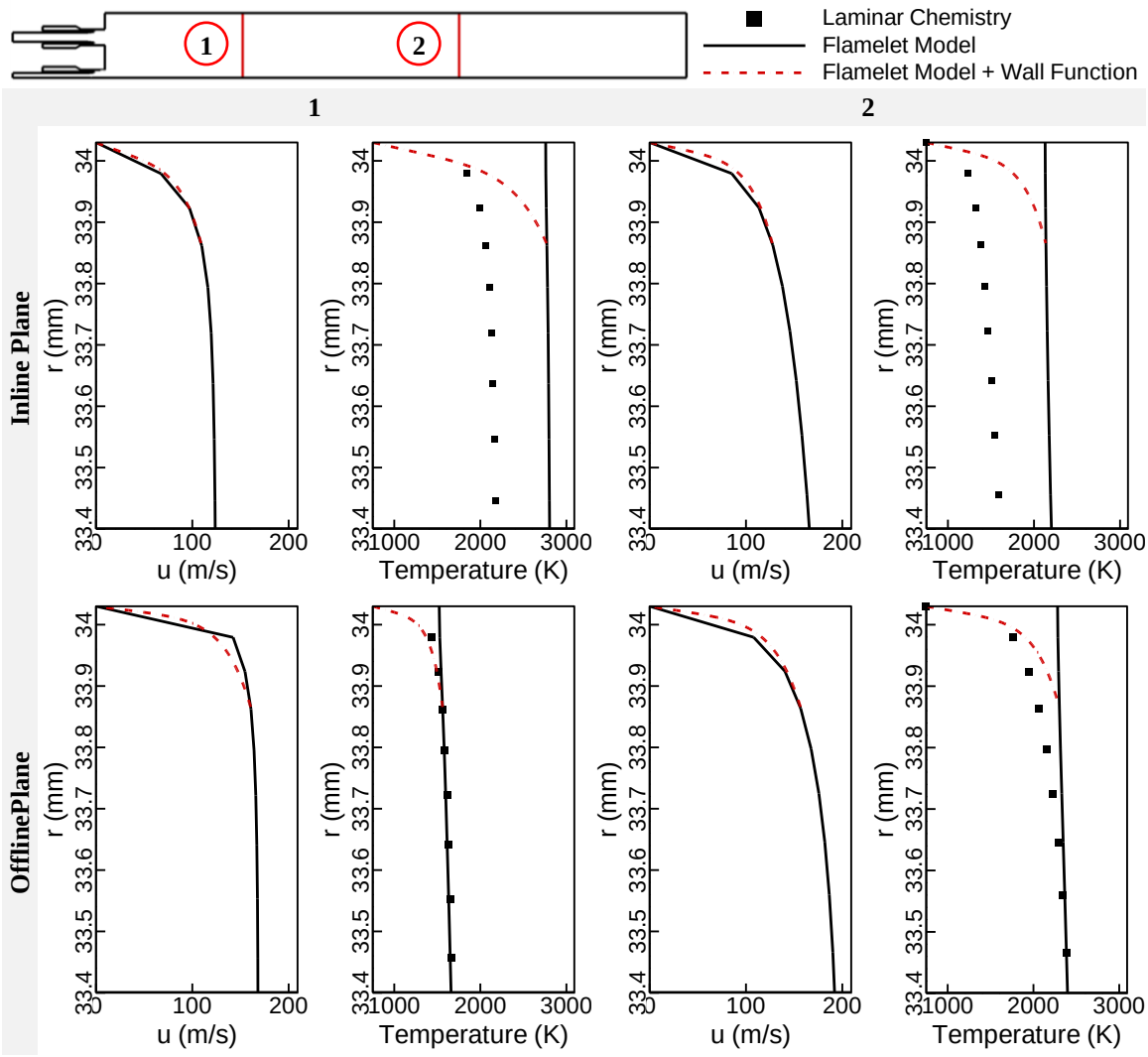

Figure 17. Radial temperature and velocity profiles at two different axial locations in the inline and offline planes. The upper range of the radial distance, r, correspond to the wall. The black symbols represent the laminar finite-rate chemistry solution and they correspond to radial grid point locations.

IV. Summary and Conclusions

Two different experimental injector setups were tested: a single element injector due to the Pal et al.[23] which was also investigated in a previous study[24] and a multi-element injector setup due to deRidder et al[28,29].

The turbulence-chemistry interaction (TCI) and non-equilibrium chemistry effects for the Pal et al.[23] injector case are investigated by comparing the adiabatic wall simulation results of the laminar finite rate chemistry (LFRC) model, the laminar flamelet model (LFM) and the presumed PDF/equilibrium model (flamelet model with $\chi = 0$).

The non-equilibrium chemistry effect was shown to be unimportant consistent with previous results[24] obtained using LFRC in which different chemistry mechanisms were shown to have no noticeable impact on the solution and based on the mean flow variables, chemical time scales were demonstrated to be smaller than the convective and diffusive time scales in the flow field. With the current analysis, we show that for the cases examined, the non-equilibrium chemistry effect is insignificant in the laminar flamelet model (LFM) framework. Similar to the work of Correa and Shyy[44], we find that the assumed PDF/equilibrium model is of sufficient fidelity to resolve turbulence-chemistry interaction without the need of to account for chemical non-equilibrium with the flamelet model.

The temperature profiles at several axial locations and PDF distributions at select representative points in the high shear region, recirculating region, near the chamber wall and away from the flame surface are inspected. In the

absence of the chemical non-equilibrium effects, TCI is governed by the local mean and variance of Z, in the form of an assumed PDF. The width of the PDF is determined by the mean variance of Z. Hence in regions with high variations in mixture composition coupled with highly turbulent flow, such as near the flame surface, TCI effect is prominent while it diminishes with the distance from the flame surface. In the single element injector configuration of Pal et al.[23], flame surface lies far from the wall and the TCI effect doesn't alter the wall temperature distribution significantly. However this is only due to this particular single element injector test case setup. In realistic multi-element injectors where an array of injector elements is typically placed close to the chamber wall, the turbulence-chemistry interaction may be expected to have a considerable effect in wall heat flux predictions.

A zonal wall treatment for the case of Pal et al.[23] was proposed based on previous results. Low-Re turbulence model approach is used at recirculation regions of the flow while law-of-the-wall method is used elsewhere. This treatment showed considerable improvement in the overall wall heat flux distribution profile when compared to the experimental data.

An experimental multi-element H_2/O_2 injector due to deRidder et al.[28,29] was analyzed with the laminar finite-rate chemistry (LFRC) and laminar flamelet model (LFM) with only the latter accounting for the effects of turbulence-chemistry interaction (TCI). The flamelet model, due to TCI, resulted in reduced temperatures near the stoichiometric flame surface as expected. The flamelet model predicted a thinner near wall fuel rich layer that yielded a higher near wall temperature in the inline plane compared to the laminar finite-rate chemistry model simulation results. Assuming that the heat loss effects are contained within a thin layer near the wall, a methodology based on the law-of-the-wall formulation was described for obtaining wall heat flux distribution as a post-processing step of the flamelet model. The overall wall heat flux distribution was under-predicted in the inline plane by the LFRC model. The flamelet model prediction on the other hand was in good agreement with the experimental data. In both the inline, intermediate and offline planes, both models suffered from under-predicting the experimental wall heat flux values in the upstream regions where near wall recirculation regions or large streamline curvature existed. This is due to limitations of the law-of-the-wall formulation as was shown in previous[24] and current work, and a zonal wall treatment approach may be helpful.

Acknowledgments

This study is supported by the NASA Constellation University Institute Program (CUIP), Claudia Meyer and Jeff Rybak program managers. We have benefited from collaboration with Dr. Edward A. Luke of Mississippi State University, Kevin Tucker of NASA Marshall Space Flight Center and Dr. Mauritz deRidder and Dr. William Anderson of Purdue University.

References

[1]Foust, M.J., Deshpande, M., Pal, S., Ni, T., Merkle, C.L., Santoro, R.J., "Experimental and analytical characterization of a shear coaxial combusting GO2/GH2 flowfield," AIAA-96-0646, 34th AIAA Aerospace Sciences Meeting and Exhibit, Jan 15-18, Reno, NV, 1996

[2]Venkateswaran, S., Weiss, J.M., Merkle, C.L., Choi, Y.-H., "Propulsion-related flowfields using the preconditioned Navier-Stokes equations," AIAA Paper 92-3437 , 28th AIAA/ASME/SAE/ASEE Joint Propulsion Conference and Exhibit, Nashville, TN, July, 1992.

[3]Schley, C.-A., Hagemann, G., Tucker, K.P., Venkateswaran, S., Merkle, C.L., "Comparison of computational codes for modeling hydrogen-oxygen injectors," AIAA-1997-3302, 33rd AIAA/ASME/SAE/ASEE Joint Propulsion Conference and Exhibit, Seattle, WA, July, 6-9, 1997.

[4]Schley, C.-A., Hagemann, G., Golovitchev, V., "Comparison of high pressure H2/O2 rocket model engine reference simulations," AIAA-95-2429, 31st AIAA/ASME/SAE/ASEE Joint Propulsion Conference and Exhibit, Monterey, CA, June 28-30, 1995.

[5]Chen, Y.S., "Compressible and incompressible flow computations with a pressure based method," AIAA Paper 89-0286, 27th AIAA Aerospace Sciences Meeting and Exhibit, Reno, NV, Jan. 1989.

[6]Oefelein, J.C., Yang, V., "Modeling high-pressure mixing and combustion processes in liquid rocket engines," Journal of Propulsion and Power, vol. 14, no. 5, 1998.

[7]Mayer, W., Tamura, H., "Propellant injection in a liquid oxygen/gaseous hydrogen rocket engine," Journal of Propulsion and Power, vol. 12, pp. 1137-1147, 1996.

[8]Ivancic, B., Mayer, W., "Time- and length scales of combustion in liquid rocket thrust chambers," Journal of Propulsion and Power, vol. 18, no. 2, 2002.

[9]Lin, J., West, J.S., Williams, R.W., Tucker, K.P., "CFD code validation of wall heat fluxes for a GO2/GH2 single element combustor," AIAA-2005-4524, 41st AIAA/ASME/SAE/ASEE Joint Propulsion Conference and Exhibit, Tucson, AZ, July, 10-13, 2005.

[10] Marshall, W.M., Pal, S., Woodward, R.D., Santoro, R.J., "Benchmark wall heat flux data for a GO2/GH2 single element combustor," AIAA-2005-3572, 41st AIAA/ASME/SAE/ASEE Joint Propulsion Conference and Exhibit, Tucson, AZ, July, 10-13, 2005.

[11] Luke, E.A. and George, T., "Loci : A rule-based framework for parallel multidisciplinary simulation synthesis," Journal of Functional Programming, vol. 15, no. 3, 477-502, May 2005 .

[12] Luke, E. and Cinnella, P., "Numerical simulations of mixtures of fluids using upwind algorithms," Computers & Fluids, vol. 36, no. 10, 1547-1566, doi:10.1016/j.compuid.207.03.008, 2007.

[13] Oefelein, J.C., "Numerical mixing and combustion of cryogenic oxygen-hydrogen shear-coaxial jet flames at supercritical pressure," Combust. Sci. and Tech., 178:229-252, 2006.

[14] Oschwald, M., Smith, J.J., Branam, R., Hussong, J., Schik, A., "Injection of fluids into supercritical environments," Combust. Sci. and Tech., 177:2087-2138, 2005.

[15] Cheng, G.C., Farmer, R., "Real fluid modeling of multiphase flows in liquid rocket engine combustors," Journal of Propulsion and Power, vol. 22, no. 6, 2006

[16] Vingert, L., Habiballah, M., "Test case RCM 2: cryogenic spray combustion at 10 bar at Mascotte," Proceedings of the 2nd International Workshop on Rocket Combustion Modeling, Deutsches Zentrum fur Luft-und Raumfahrt (DLR), Lampoldshausen, Germany, 2001

[17] Thomas, J.L., Zurbach, S., "Test case RCM 3:supercritical spray combustion at 60 bar at Mascotte," Proceedings of the 2nd International Workshop on Rocket Combustion Modeling, Deutsches Zentrum fur Luft-und Raumfahrt (DLR), Lampoldshausen, Germany, 2001

[18] Mack, Y., Haftka, R., Segal, C., Queipo, N., Shyy, W., "Computational modeling and sensitivity evaluation of liquid rocket injector flow," AIAA-2007-5592, 43rd AIAA/ASME/SAE/ASEE Joint Propulsion Conference and Exhibit, Cincinnati, OH, July, 8-11, 2007.

[19] Conley, A., Vaidyanathan, A., Segal, C., "Heat flux measurements in a GH2/GO2 single-element injector," AIAA-2006-5048, 42nd AIAA/ASME/SAE/ASEE Joint Propulsion Conference and Exhibit, Sacramento, CA, July, 9-12, 2006.

[20] Thakur, S. and Wright, J., "Validation of a pressure-based combustion simulation tool for a single element injector test problem," 3rd International Workshop on Rocket Combustion Modeling, Paris, France, March 13-15, 2006.

[21] Thakur, S., Wright, J. and Shyy, W., "An Algorithm for Chemically Reacting Flows on Generalized Grids Using a Rule-Based Framework," 43rd AIAA Conference, Paper No. 2005-0875, Reno, NV (Jan 2005).

[22] Tucker, P.K, Menon, S., Merkle, C.L., Oefelein, J.C., Yang, V., "Validation of high-fidelity CFD simulations for rocket injector design," AIAA-2008-5226, 44th AIAA/ASME/SAE/ASEE Joint Propulsion Conference and Exhibit, Hartfrod, CT, July, 21-23, 2008.

[23] Pal, S., Marshall, W., Woodward, R., Santoro, R., "Wall heat flux measurements for a uni-element GO2/GH2 shear coaxial injector," Third International Workshop on Rocket Combustion Modeling, Paris, France, March, 13-15, 2006.

[24] Sozer, E., Vaidyanathan, A., Segal, C., and Shyy, W., "Computational Assessment of Gaseous Reacting Flows in Single Element Injector", AIAA-2009-449, 47th AIAA Aerospace Sciences, Orlando, Florida, Jan. 5-8, 2009.

[25] Vaidyanathan, A., Gustavson, J., Segal, C. "Heat fluxes/OH PLIF measurements in a GO2/GH2 single-element, shear injector," AIAA-2007-5591, 43rd AIAA/ASME/SAE/ASEE Joint Propulsion Conference and Exhibit, Cincinnati, OH, July, 8-11, 2007.

[26] Menter, F.R., "Two-Equation Eddy-Viscosity Turbulence Models for Engineering Applications," AIAA J., Vol. 32, No. 8, pp 269-289 (1994).

[27] Menter, F. R., Kuntz, M., and Langtry, R., "Ten Years of Industrial Experience with the SST Turbulence Model," Turbulence, Heat and Mass Transfer 4, ed: K. Hanjalic, Y. Nagano, and M. Tummers, Begell House, Inc., pp. 625 – 632 (2003).

[28] deRidder, M. A., Helderman, D. A., Nugent, N. J., Anderson, W. E., "Measurement and Analysis of Heat Transfer in a Multi-Element Hydrogen/Oxygen Rocket Combustor", 44th AIAA/ASME/SAE/ASEE Joint Propulsion Conference & Exhibit, 21-23 July 2008, Hartford, CT, AIAA 2008-5031.

[29] deRidder, M. A., Anderson, W.E., "Heat Flux and Pressure Profiles in a Hydrogen /Oxygen Multielement Rocket Combustor", to be published.

[30] Nichols, R.H., Nelson, C.C., "Wall Function Boundary Conditions Including Heat Transfer and Compressibility", AIAA Journal, 42, pp. 1107-1114, 2004.

[31] Evans, J.S., Schexnayder, C.J., "Influence and chemical kinetics and unmixedness on burning in supersonic hydrogen flames," *AIAA Journal*, vol. 18, no. 2, pp. 188-193, 1980.

[32] Peters, N., "Local quenching of diffusion flamelets and non-premixed turbulent combustion", Combust. Sci. Technol., 30, 1, 1983, first published as Western States Section of the Combustion Institute, paper WSS 80-4, Spring Meeting, Irvine, CA, 1980.

[33] Peters, N., "Laminar Diffusion Flamelet models in Non-premixed Turbulent Combustion", Prog. Energy Combust Sci., 10, 319-339, 1984.

[34] Janicka, J., Peters, N., "Prediction of Turbulent Jet Diffusion Flame Lift-off Using a PDF Transport Equation", 19th Symp. (Int.) on Combustion, pp. 367-374, The Combustion Institute, Pittsburg, 1982.

[35] Jones, W. P. and Whitelaw, J. H. "Modeling and measurements in turbulent combustion", 20th Symp. Int'l on Combustion, pp. 233-249 The Combustion Institute, 1984

[36] Libby, P.A. and Williams, F. A. (Eds), "Turbulent Reacting Flows" Springer-Verlag, New York ,1980

[37] Williams, F.A., "Recent advances in theoretical descriptions at turbulent diffusion flames", Turbulent Mixing in Nonreactive and Reactive Flows, pp189-208, 1975

[38] Jones, W. P. and Whitelaw, J. H. "Modeling and measurements in turbulent combustion", 20th Symp. Int'l on Combustion, pp. 233-249 The Combustion Institute, 1984

[39] Williams, F.A. "Asymptotic methods in turbulent combustion", AIAA paper 84-0475, Reno, Nevada 1984

[40] Liew, S.K., Bray, K.M.C. and Moss, J. B "A flamelet model of turbulent non-premixed combustion", Combust. Sci Technol. 27, 69-73, 1981

[41] Kent, J. H. and Bilger, R. W. ,"The Prediction of turbulent diffusion flame fields and nitric oxide formation",16th Symp. Int'l on Combustion,pp1643-1656, The Combustion Institute, 1976

[42] Peters, N., "Turbulent Combustion", Cambridge University Press, 2000.

[43] Barlow, R.S., Dibble, R.W., Chen, J.-Y., Lucht, R.P., " Effect of the Damkohler number on super-equilibrium OH concentration in turbulent nonpremixed jet flames", Combustion & Flame, vol. 82, pp. 235-251, 1990.

[44] Correa, S.M and Shyy, W., "Computational models and methods for continuous gaseous turbulent combustion" Prog. Energy combust. Sci, vol 13, pp249-292, 1987.

[45] Kuo, K.K., "Principles of Turbulent Combustion", 2nd edition, Wiley, 2005.

[46] White, W.B., Johnson, S.M., Dantzig, G.B., "Chemical Equilibrium in Complex Mixtures", J. Chem. Phys., 28, 751, 1958.

[47] Gibson, C.H., Massiello, P.J., "Statistical Models and Turbulence", Rosenblatt, M., Van Atta, C., editors, Lecture Notes in Physics, 12, pp. 427, Springer, 1972.

[48] Antonia, R.A., Sreenivasan, K.R., "Log-normality of Temperature Dissipation in a Turbulent Boundary Layer", Phys. Fluids, 20, 1800, 1977.

[49] Effesberg, E., Peters, N., "Scalar Dissipation Rates in Turbulent Jets and Jet Diffusion Flames", 22nd Symp. (Int.) on Combustion, The Combustion Institute, Pittsburg, pp. 693-700, 1988.